# **CAAP Annual Report**

**Date of Report**: 09/30/2025

**Prepared for**: U.S. DOT Pipeline and Hazardous Materials Safety Administration

**Annual Period:** From October, 1, 2024 to September, 30, 2025

**Contract Number**: 693JK32350001CAAP

**Project Title**: Rhamnolipid: a Bio-based, Ecologically Friendly, Corrosion Inhibitor and

SRB Biocide for Crude Pipelines

**Prepared by:** Scott Lillard

Contact Info.: <u>rsl@uakron.edu</u>, 330-972-7463

# **Table of Contents**

Table	of Con	tents	2
Section	on A: B	usiness and Activities	3
	(a)	Contract Activities	3
	(b)	Financial Summary	3
	(c)	Project Schedule Update	3
	(d)	Work with Cost Share Partners	4
Section	on B: D	etailed Technical Results in the Report Period	5
1.	Backg	ground and Objectives in the 2nd Annual Report Period	5
	1.1.	Background	. 5
	1.2.	Objectives in the 2nd Annual Report Period	. 5
2.	Exper	imental Program in the 2nd Annual Report Period	5
	2.1.	RhL Production	5
	2.2.	RCE Expereiments	6
	2.3.	RhL Production	7
	2.4.	MIC	8
3.	Results and Discussions		
	3.1.	Task 1: RhL Fermentation	11
	3.2.	Task 2: Inhibition Mechanism and % Saline Effects	14
	3.3.	Task 3: MIC	20

## **Section A: Business and Activities**

### (a) Contract Activities

- Contract Modifications:
  - None to report
- Educational Activities:
  - Student mentoring:
    - Graduate Students: Uddipta Mondal, B.S. Chem. Eng., BUET, Tijani Abdul-Gafaru B.S. Petroleum Eng., Kwame Univ., Gahana; Elaheh Mozayan, M.S. Biochem., University of Kashan, Iran; Kingsford Duah Agyemang, B.S. Petroleum Eng., Kwame Univ., Gahana.
    - Undergrad Honors Projects: Elizabeth Zimmerer (Chem. Eng.), Rosemary Sterling (Chem. Eng.)
  - Student internship:
    - Undergrads: Calli Lewis, Lily Clemente, Jack Schultz.
  - o Educational activities:
    - None to report
  - Career employed:
    - None to report
- Dissemination of Project Outcomes:
  - None to report

### (b) Financial Summary

- Federal Cost Activities:
  - o Total Budget:
    - Total Direct and Indirect: \$502,888.4
  - o PI/Co-PIs/students involvement:
    - **\$190,523.57**
  - o Materials purchased/travel/contractual:
    - **\$7,104.23**
- Cost Share Activities:
  - o Cost share contribution: \$52,901.61

### (c) Project Schedule Update

• Project Schedule:

Task 1: Corrosion Inhibition Efficiency (IE)

- o a) IE in Produced Water Surrogate (PWS): 90% complete
- o b) IE in Crude Surrogate (CS): 15% Complete
- o c) IE in Crude: Oct '25 delayed to Jan '26.

Task 2: Microbial Influenced Corrosion (MIC)

- o a) RhL as an SRB-MIC Biocide in PWS: 50% complete.
- o b) RhL as an SRB-MIC Biocide in CS: delayed to Jan '26.
- o c) Cell Attachment in PWS: Apr '25 delayed to Jan '26...

### Task 3: RHL Production and Comparison of Di-RhL vs. Mono-RhL in PWS

- o a) RhL Production (Fermentation): 50% complete
- o b) Initial Separation of Di-RhL and Mono-RhL: delayed to Jan '26.
- o c) IE in PWS: Jan '25 Dec '25 10% complete.
- Corrective Actions:
  - None to report

### (d) Work with Cost Share Partners

We have been working with BP America (PI: Dr. Shokrollah Hasani) on four fronts: 1) shipment of produced water (PW) from Eagle Ford and corresponding chemical analysis, 2) shipment of crude from Eagle Ford, 3) qualification's necessary for inhibitor service and 4) site visit to Eagle Ford. BP has shipped Eagle Ford PW samples. Prior to testing in these samples, we have first measured RhL inhibition efficiency at saline concentrations comparable to Eagle Ford (see below, complete). We have begun tests in in a simulant based on the water chemistry analysis (to be reported on in FY '26 Q1) and anticipate completing the Eagle Ford PW tests in Q1. We also anticipate an Eagle Ford site visit in FY '26 Q1.

# Section B: Detailed Technical Results in the Report Period

# 1. Background and Objectives in the 2<sup>nd</sup> Annual Report Period

### 1.1. Background

This project is focused on a novel biobased surfactant, rhamnolipid, as a corrosion inhibitor and sulfate reducing bacteria (SRB) biocide for crude pipelines. Rhamnolipids (RhL) are a group of glycolipids produced by bacteria, here by *Pseudomonas aeruginosa*, that are biodegradable, ecologically acceptable, and renewable. From a corrosion engineering standpoint, there is evidence from our past work that RhLs inhibit corrosion and reduce SRB attachment. To evaluate the application of RhLs to crude pipelines we propose to: 1-Determine the critical concentration of RhL necessary for corrosion inhibition / SRB mitigation in an oil field produced water simulant, 2- Evaluate whether or not one RhL structure (mono vs. di) is a better inhibitor or if a mixture of the two is better, 3- Evaluate how the presence of an organic phase that simulates the crude affects RhL partitioning between the organic and aqueous phases and, ultimately, corrosion inhibition, and 4 – Validate our results by making measurements in actual crude samples.

## 1.2. Objectives

This project will answer the question: Can RhLs be used as a corrosion inhibitor and SRB biocide for crude oil pipelines? To accomplish this goal, we will undertake four main tasks: 1- Determine the critical concentration of RhL necessary for corrosion inhibition / SRB mitigation in an oil field produced water simulant, 2- Evaluate whether or not one RhL structure (mono vs. di) is a better inhibitor or if a mixture of the two is better, 3- Evaluate how the presence of an organic phase that simulates the crude affects RhL partitioning between the organic and aqueous phase and, ultimately, corrosion inhibition, and 4 – Validate our results by making measurements in actual crude samples to determine if variables such as mass% water, sulfur content, total acid number and API gravity, etc. affect the inhibition efficiency of RhL. The goals of FY '25 were to a) ferment *Pseudomonas aeruginosa* at UA, harvest RhL and quantify the purity b) explore the mechanism of corrosion inhibition efficiency of RhL using electrochemical impedance spectroscopy (EIS) and quartz crystal microbalance (QCM), begin MIC-SRB testing (immersion & electrochemical).

# 2. Experimental Program in the 2<sup>nd</sup> Annual Report Period

#### 2.1. RhL Production

Rhamnolipid was produced from the bacteria, *Pseudonymous aeruginos*a using an existing frozen strain in our lab. The bacteria were activated by transferring 1.5 mL of a glycerol-preserved culture to 10 mL of 30 g/L tryptic soy broth (TSB) and incubating it at 32°C for 12 h in an orbital shaker operating at 150 rpm. The activated culture was added to 90 mL TSB

and grown at the same condition for 20 h before being used as the seed culture for fermentation. The fermentation was carried out in a 3 L fermentor with 1 L initial medium containing 100 g soybean oil, 2.51 g nitrogen (from NH4Cl, yeast extract and peptone) and other nutrients in deionized water. The fermentor was equipped with probes, pumps, and other equipment to control the temperature (32°C), pH, foaming, and dissolved oxygen concentration. Prior to reactor start-up, the system was autoclaved at 250°F for 20 minutes and then cooled to room temperature. The fermentor was then inoculated with 100 mL seed culture. The dissolved oxygen concentration was controlled with a set point of 10% air saturation (about 0.8 mg O<sub>2</sub>/L) by addition of pure O<sub>2</sub> as needed. pH was allowed to drop initially from 7 to 5.7 and was then controlled at that level by addition of 1N NaOH and H<sub>2</sub>SO<sub>4</sub>. The medium was agitated at 800 rpm with two sets of 6-blade Rushton turbines. In addition to the nutrients in the initial medium, soybean oil was continuously added at the rate of 0.83 g/(L-h) throughout the fermentation, and a 300 g/L NH<sub>4</sub>NO<sub>3</sub> solution was added at 2.00 g/(L-h) during 15-41 h and then at 0.15 g/(L-h) untill the end of fermentation.

### 2.2. RCE Experiments

Potentiodynamic polarization curves for C1018 carbon steel in a rotating cylinder electrode setup (1000 rpm) were generated to assess the corrosion current density (proportional to corrosion rate) as a function of rhamnolipid (RhL) concentration. The base solution was a 1% NaCl solution saturated with CO<sub>2</sub> and was chosen as it is the most aggressive produced water simulant known as well as having system properties that are well characterize. Once prepared, the solution was placed in a water-jacketed cell to maintain temperature (30 °C) and subsequently purged with CO<sub>2</sub> for up to 12 hrs. This cell also contained a graphite counter electrode and SCE reference electrode. The C1018 specimen was ground to silicon carbide 600 grit to provide a reproducible surface finish. After grinding, the specimen was ultrasonically cleaned in successive baths acetone, ethanol and DI water followed by drying with CO<sub>2</sub>. The initial RhL concentration test was typically 0.01 mass/volume % (100 ppm). All experiments were run in duplicate to insure reproducibility. A diagram of this set up is presented in Figure 2.1. The set-up was used for to generate open circtuit potential data, potentiodynmaic polarization curves, linear polarization resistance (LPR) data and electrochemical impedance spectroscopy (EIS) data.

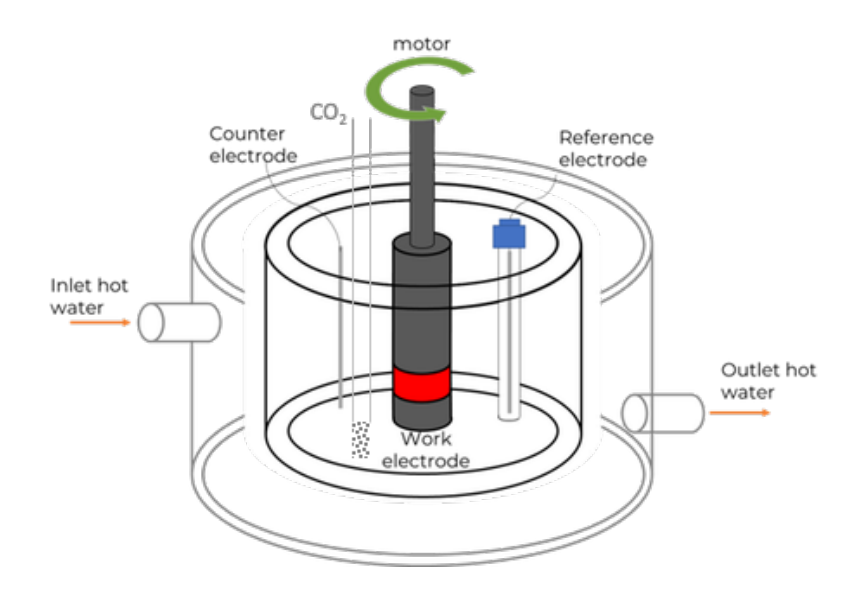


**Figure 2.1** Temperature controlled electrochemical cell (jacketed) used for Rotating Cylinder Electrode experiments.

### 2.3. QCM.

A quartz crystal microbalance (QCM) measures the mass adsorbed onto the surface of a quartz crystal by quantifying resonant frequency shifts of the quartz crystal. The objective of this research project is to determine the mass of RhL adsorbed onto surfaces as a function of solution composition (pH, salinity). The relationship between mass and resonant frequency is given by:

$$\Delta m = -\frac{C\Delta F}{n}$$

where  $\Delta m = \text{mass variation per area of the sensor (ng/cm}^2)$ ,  $\Delta F = \text{variation of frequency (Hz)}$ ,  $C = \text{a constant (17.8 ng/cm}^2\text{-Hz)}$  and n = harmonic number (1,3,5,7...13).

The QCM used for this project is the electrochemical quartz crystal microbalance (eQCM) 15 M from Gamry Instruments. Data collection is performed on the Gamry Resonator software 7.10.4. The elelectrochemical flow-cell used in these experiments contained traditional working (WE), counter (CE) and reference (RE) electrodes alloying for real-time EIS and LPR data. Solution was flowed through the cell using a peristaltic pump (**Figure 2.2**) and the cell and solution flowing into it was maintained at 30 °C. The pump had multiple channels which allowed for solutions without and with RhL to be flowed the cell at separate intervals via a 4-way valve. Here, experiments are reported for two buffer solutions, pH 8 phosphate buffer solution (**Table 2.1**) and a pH 4 acetic acid buffer (**Table 2.2**).

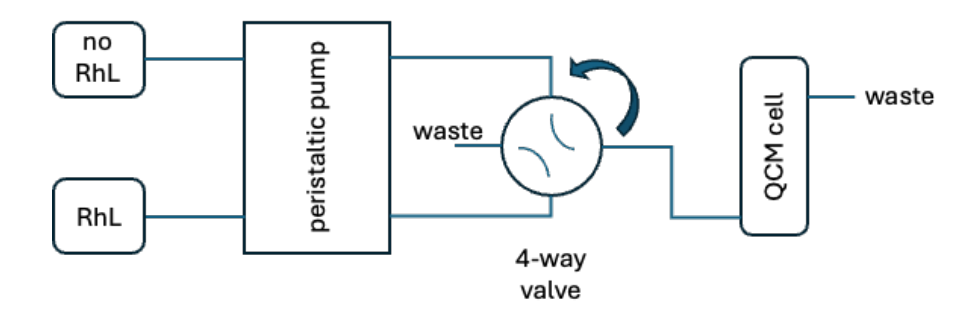


**Figure 2.2** Temperature controlled electrochemical flow-cell used for Quartz Crystal Microbalance experiments.

**Table 2.1:** Composition of the pH 8 phosphate buffer solution use in the QCM experiments.

	Form	w/o rhl	w/ rhl
Sodium Dihydrogen Phosphate	Powder	69 g	69 g
Sodium Phosphate Dibasic	Powder	71 g	71 g
Rhamno Lipid	Viscous Liquid	0 mL	16.8 mL

**Table 2.2:** Composition of the pH 4 acetic acid buffer solution use in the QCM experiments.

	Form	w/o rhl	w/ rhl
0.6 M Potassium Acetate	Stock Soln	43.5 mL	43.5 mL
0.6 M Acetic Acid	Stock Soln	13.0 mL	13.0 mL
Rhamno Lipid	Viscous Liquid	0 mL	1.68 mL

#### 2.4. MIC

American Type Culture Collection 7757 was cultured in two anaerobic test solutions:

Postgate medium C. One liter of this medium contains 6 g sodium pyruvate (C<sub>3</sub>H<sub>3</sub>NaOs), 4.5 g sodium sulfate (Na<sub>2</sub>SO<sub>4</sub>), 1 g yeast extract, 1 g ammonium chloride (NH<sub>4</sub>Cl), 0.5 g monopotassium phosphate (KH<sub>2</sub>PO<sub>2</sub>), 0.3 g sodium citrate dihydrate (Na<sub>3</sub>C<sub>3</sub>H<sub>3</sub>O<sub>7</sub>-2H<sub>2</sub>O), 0.06 g magnesium sulfate heptahydrate (MgSO<sub>4</sub>-7H<sub>2</sub>O), 0.04 g calcium chloride hexahydrate (CaCl<sub>2</sub>-6H<sub>2</sub>O), 0.004 g ferrous sulfate heptahydrate (FeSO<sub>3</sub>-7H<sub>2</sub>O) and a cysteine stock solution to achieve a final concentration of 0.002 g/l. The pH is adjusted to 7.0 by addition of 1 M NaOH solution.

Modified Baar's. One liter of this medium contains 1g sodium lactate, 0.25g ammonium

chloride, 1.25g sodium citrate dihydrate, 0.5g magnesium sulfate, 0.25g calcium sulfate, 0.84g sodium bicarbonate and 10g NaCl.

Prior to culturing the bacteria, 5ml of ATCC 1249 was dispensed into different sterilized serum bottles via sterilized pipette using an anaerobic chamber. The serum bottles were covered with sterilized butyl stoppers. The serum bottles were capped with aluminum covers to make it airtight. Each serum bottle was then dosed with 0.2ml of 100mM sodium sulfide  $(Na_2S)$  was added to. The medium turned pink and colorless within 3mins indicating a complete anaerobic environment. Prior to the addition of the  $Na_2S$ , the sterilized needle and syringe were purged with nitrogen, and the cap of the serum bottle was sterilized with ethanol. The serum bottles were put back into the anaerobic chamber.

Once the serum bottles were prepared, the supplier's bacteria vial was heated over a Bunsen burner and squirted with DI water to crack the glass. The vial was transferred into the anaerobic chamber and then broken to retrieve the content. A sterilized tweezer was used to offload the content from the vial. A sterilized syringe was used to transfer 0.5ml of ATCC 1249 into the inner vial to rehydrate the freeze-dried bacteria. The content was transferred into a pre-reduced 10ml vial containing 5ml of ATCC 1249. The inoculated medium was incubated at 37°C.

In one set of experiments, 30-day exposure tests were conducted and corrosion rate was assessed via mass loss. For these corrosion experiments, C1018 corrosion rate in the test with and without RhL In these experiments, C1018 specimens were ground to 600 grit SiC and cleaned using acetone/ethanol/DI water in an ultrasonic cleaner. The mass of the specimens was then recorded. Modified Baar's was then prepared and subsequently sterilized, along with all other glassware by autoclaving at 121 °C for 20 min. Argon was bubbled through the medium overnight (12 hr. min.) to remove O2 prior to inserting the C1018 specimens. In this procedure a 0.2 µm filter was used to sterilize the Ar gas. The C1018 steel specimens, attached to bottle caps specifically designed for these types of exposure experiments, were transferred to the media bottles in a glove bag that was also purged with Ar. The specimens were hung from a bottle cap especially design for immersion test (Figure 2.3). To unsure a good seal (and limit O2 diffusion into the bottle), the bottle threads were first sealed with PTFE tape. Additionally, the out die of the bottle cap was sealed with Parafilm.



**Figure 2.3** The deaeration set-up used 30 day immersion tests. Threads were sealed with PTFE tape and the cap was covered with parafilm.

The electrochemical set-up for real time electrochemical experiments with and without RhL is presented in **Figure 2.4**. Both cells contained 500 mL of the test solution. For deaeration to occur, the cells must be completely sealed except for the inlet and outlet. To ensure CO<sub>2</sub> was being properly flushed through, the pressure differential was checked via small flasks of water. If bubbling was observed, CO<sub>2</sub> flow was sufficient for proper deaeration.

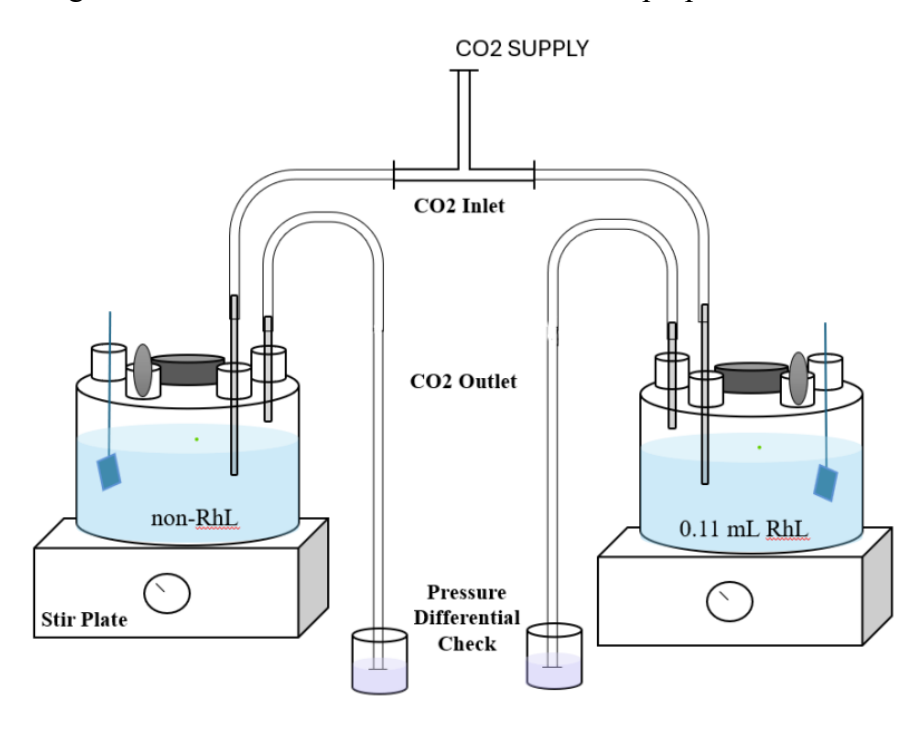


**Figure 2.4** The deaeration set-up used for 24 hours before the 4-day exposure period. All orifices were sealed with rubber stoppers, aluminum foil (shown as the gray ovals above), and parafilm.

#### 3. Results and Discussions

#### 3.1. Task 1: RhL Fermentation

Improved Dissolved Oxygen Control: The fermentation setup was largely unchanged from previous reports, but a major improvement was made in dissolved oxygen (DO) management. In earlier fermentations, the DO control setpoint was fixed at 10%, with an automatic on/off supply of pure oxygen. However, frequent manual adjustments to the O<sub>2</sub> flow rate were required to maintain DO levels between 5% and 100% saturation. This approach often resulted in severe DO fluctuations, including both undershooting and overshooting, especially during the fermentation phases of more dynamic changes.

To address this, we implemented a dual-line oxygen delivery system. A lean oxygen flow line was introduced to meet basal oxygen demands gradually. When the DO level dropped below the setpoint, a control algorithm activated the main oxygen line by fully opening its valve. This two-tiered approach allowed for more stable DO control, particularly during the exponential growth phase when oxygen demand surged.

However, as broth viscosity rose, the mixing efficiency deteriorated to exacerbate DO fluctuations, particularly in the stationary phase. During this phase, even the highest possible impeller rotation speeds could not sufficiently mix the broth to maintain consistent oxygenation. Moreover, the fermentor's DO sensor began to exhibit feedback delays, further complicating control. To resolve this, we integrated the Bio-Command software with condition-based logic programming. This system dynamically adjusted the lean oxygen flow and DO setpoint in response to changes in cell growth, broth rheology, and oxygen uptake rate. The improved control strategy significantly reduced both undershooting and overshooting. We will implement and further improve this control algorithm in future fermentation. The resulting DO profile in this run is illustrated in **Figure 3.1.1**.

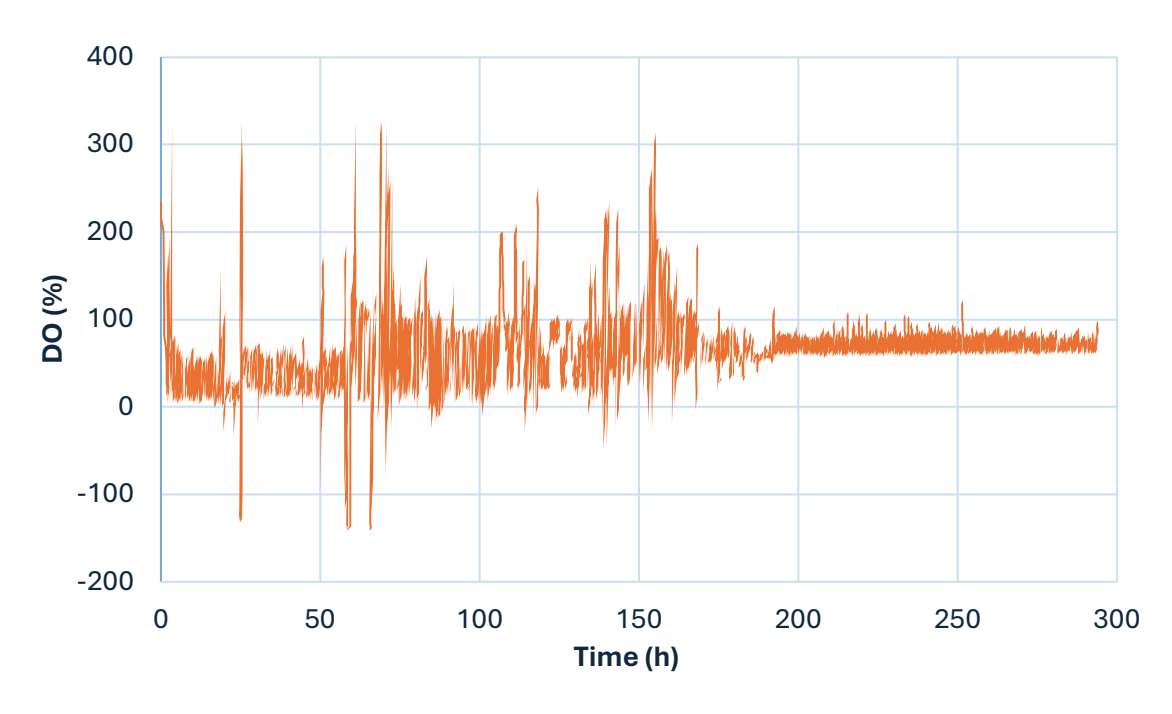


Figure 3.1.1: Dissolved oxygen (DO) concentration profile.

Improved pH and oil feed control: In the previous run, pH remained beyond the setpoint for a long period due to insufficient addition of soybean oil as the carbon source. In this run, we increased the initial oil feed rate by 50%. But it was still insufficient to support the cells' exponential growth, as indicated by the rapid pH increase after about 22 h. Later we implemented a dynamic control logic to track and adjust oil feed rate based on pH behavior. This change helped maintain the process near the target pH of 5.7, as illustrated in **Figure 3.1.2**.

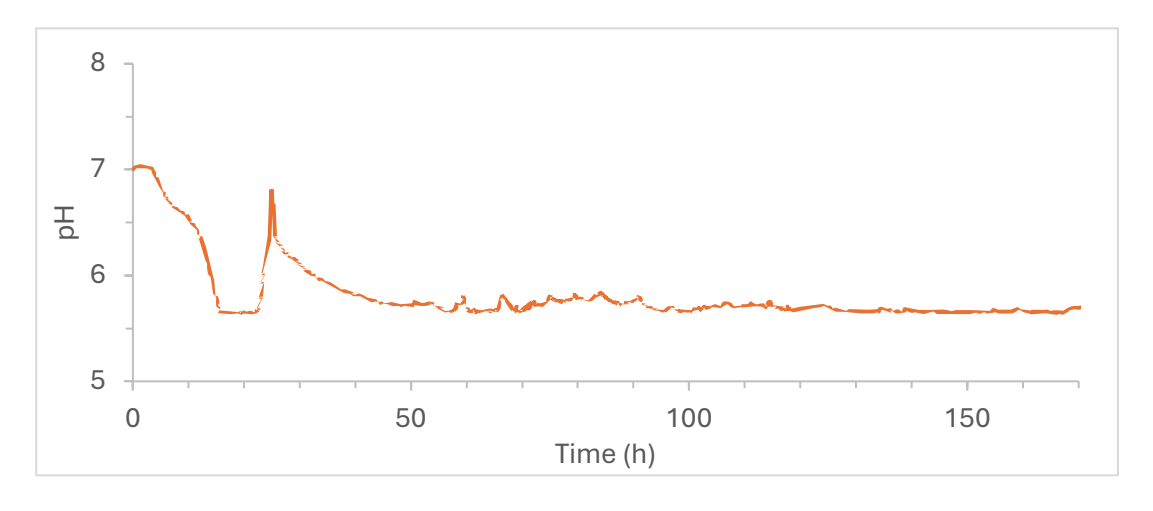


Figure 3.1.2 pH profile

Increased RhL production: This run achieved a 4.5-fold increase in RhL concentration compared to previous fermentations, reaching a peak of  $71 \pm 3$  g/L. In contrast to earlier quantification methods that relied solely on cell-free supernatants, which likely underestimated total RhL due to precipitation near its pKa, this run employed diluted raw broth for anthrone analysis, capturing both soluble and precipitated fractions. The RhL production trend over time is shown in **Figure 3.1.3.** 

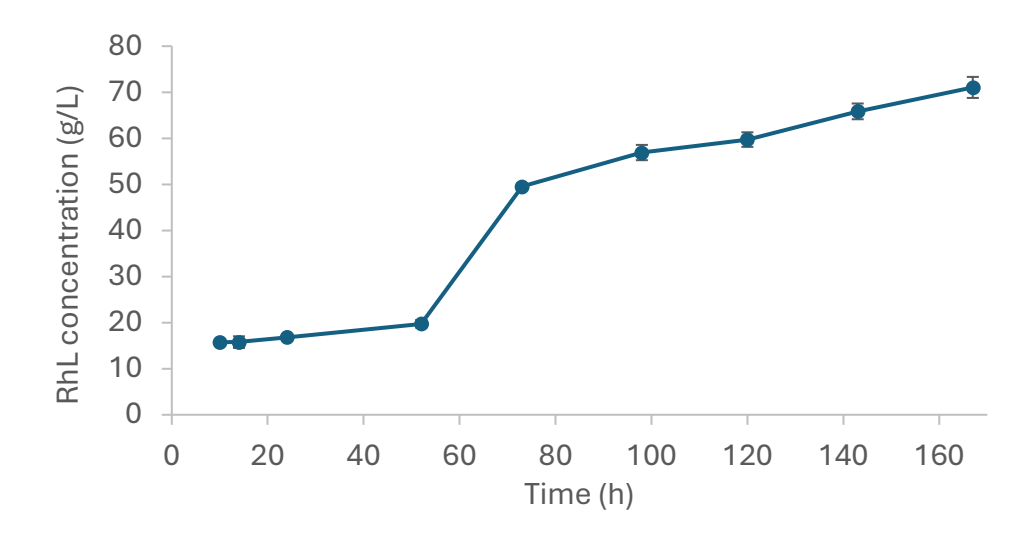


Figure 3.1.3 RhL production profile

Cell growth was monitored through intracellular protein (IP) measurements, from which cell dry weight (CDW) was estimated using an established conversion factor. These growth profiles are presented in **Figure 3.1.4**. Extended tracking of biomass concentrations beyond the feeding phase was performed to observe the decline in cell viability and biomass once oil addition ceased. This allowed for evaluation of the system's sensitivity to harvest timing.

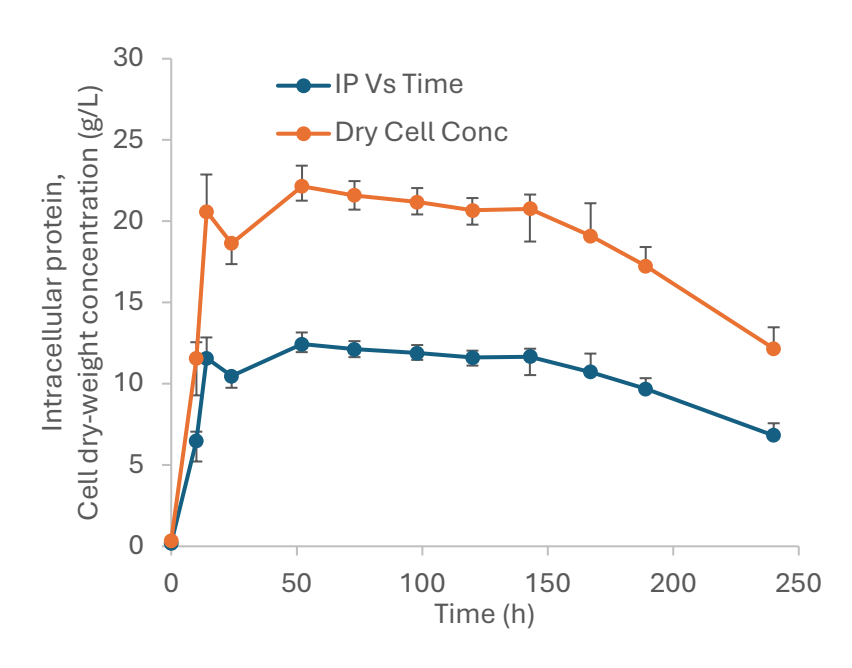


Figure 3.1.4 Profiles for intercellular protein (IP) and cell dry-weight (CDW) concentrations

### **3.2. Task 2:** *Inhibition Mechanism and % Saline Effects*

Inhibition Mechanism - EIS Signature for RhL: We have collected long-term exposure data for C1018 specimens in a produced water simulant (1% NaCl, RCE 1000 RPM, CO<sub>2</sub> purged) with and without RhL. In these experiements we are recording OCP data, polarization resistance via LPR measurements as well as polarization resistance via EIS data at E<sub>corr</sub>. In the previous quarterly report (FY '25, Q1), we discussed the LPR results for the RhL and non-RhL cases. Here we discuss our initial analysis of the EIS data in the absence of RhL while the EIS data for solutions with RhL will be discussed in the next report.

A typical Nyquist plot from the EIS vs. time data in presented in **Figure 3.2.1** which plots the imaginary impedance (Z") vs. real impedance (Z'). The data are characterized by a capacitive loop at high frequencies ( $Z = -1/j\omega C$ ) and an inductive loop at low frequencies ( $Z = j\omega L$ ). Similar data has been obtained by other investigators for steel in NaCl / CO<sub>2</sub> (Zeng, Lillard, Cong: *Corrosion* 2016). The data in **Figure 3.2.1** can be modeled by the equivalent circuit shown in **Figure 3.2.2** where:  $R_s$  is equal the geometric solution resistance between the specimen and reference electrode,  $C_{dl}$  is the double layer capacitance associated with the electrochemical interface,  $R_t$  and  $R_L$  are charge transfer resistances associated with iron oxidation and L is an inductance associated with surface adsorption of the intermediate species who's charge transfer resistance is associated with  $R_L$ . Specifically, for the CO<sub>2</sub> system  $R_t$  is proportional to the oxidation of Fe(M) to Fe(I) via the reaction:

$$Fe(M) + HCO_3^-_{ads} \rightarrow FeHCO_3^-_{ads} + e^-$$

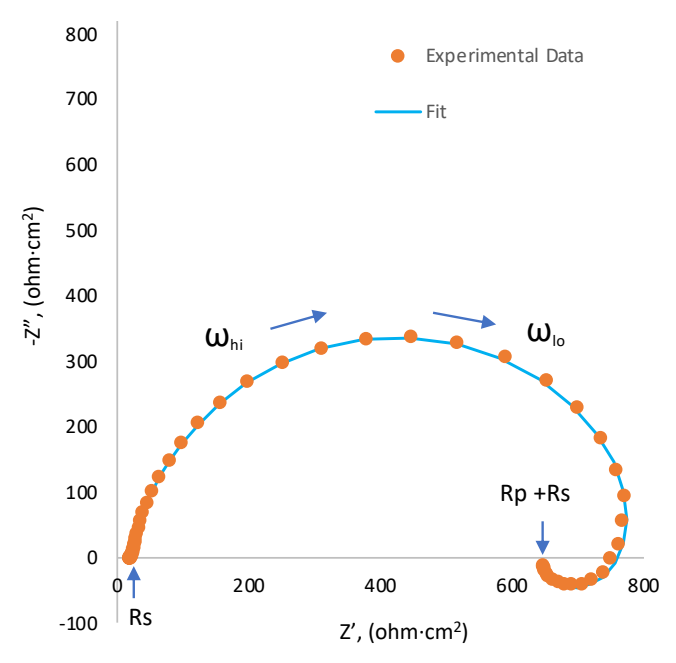


**Figure 3.2.1** Typical Nyquist plot obtained from the EIS vs time data (here, at=12 hrs.) for C1018 steel in a RCE experiment at 1000 RPM. Solution was 1% NaCl saturated with CO<sub>2</sub>. CNLS fit is also shown. The data were collected over the frequency range of 100 kHz to 0.01 Hz; in the figure, high frequencies ( $\omega$ ) are to the left and low frequencies are to the right. Graphical values for R<sub>p</sub> and R<sub>s</sub> are also shown.

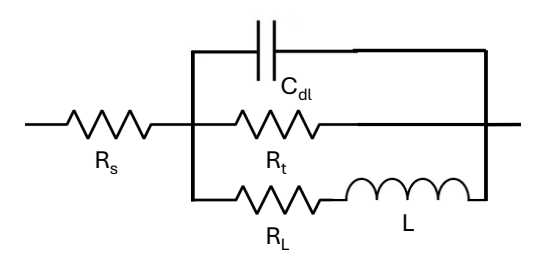


**Figure 3.2.2** Equivalent circuit model used to fit the EIS data for the non-RhL case. Elements are defined in the text.

while L and RL are associated with the accumulation of adsorbed Fe(I) carbonate and its oxidation to Fe(II) via the reaction:

$$FeHCO_3^-ads \rightarrow FeHCO_3^+ + e^-$$

A fit of the experimental data to the equivalent circuit in **Figure 3.2.2** is also presented in **Figure 3.2.1** and a summary of the values from all of the experiments are presented in **Table 3.2.1**. The polarization resistance,  $R_p$  (inversely proportional to the corrosion rate), in **Table 3.2.1** was calculated from the EIS fit using the relationship:

$$\frac{1}{R_p} = \frac{1}{R_t} + \frac{1}{R_L} \ .$$

Also in **Table 3.2.1**, the values obtained for  $R_p$  from EIS are compared with those obtained from LPR (reported on in Q1 FY '25). As seen in this table, good agreement exists between the two separate methods.

**Table 3.2.1:** Values obtained from CNLS fitting experimental EIS data vs. time to the equivalent circuit in **Figure 3.2.2**.

Fitted		1% NaCl			
parameter	t = 0  hr	t = 6hrs	t = 12 hrs	t = 18 hrs	
$R_s(\Omega \cdot cm^2)$	18.6	18.7	19.45	19.30	
$R_t(\Omega \cdot cm^2)$	296.8	684.3	819.7	829.2	
$R_L(\Omega \cdot cm^2)$	859.5	1503	2669	4363	
$C_{\rm dl}(\mu F/cm^2)$	185.2	105.1	129	154.2	
$L(\Omega \cdot cm^2)$	1263	1488	3353	6267	
$\mathbf{Rp^{EIS}}(\Omega \cdot cm^2)$	219. 8	469.6	627.1	696.76	
$\mathbf{Rp}^{\mathbf{LPR}}(\Omega \cdot cm^2)$	201.4	460.3	617.6	691.7	

For comparison to the data without RhL, EIS data were also collected for C1018 in 1% NaCl with approximately 100 ppm Rhl. The corresponding Nyquist plot is presented in **Figure 3.2.3**. Ass seen in this figure, the data are characterized by a higher frequency capacitance loop and an undetermined lower frequency response. The low frequency response being clearly different than that measured for the non-RhL solution. While we have yet to determine an electrical equivalent circuit model for this behavior (analogous to **Figure 3.2.2**), the addition of RhL has clearly increased the x intercept (Z<sub>real</sub>) at high frequencies by a factor of 10 indicating an increase in corrosion resistance. It is also noted that the low frequency inductive loop is missing, indicating RhL addition displaces water from the C1018 surface. Additional analysis will be performed on this in FY '26 Q1.

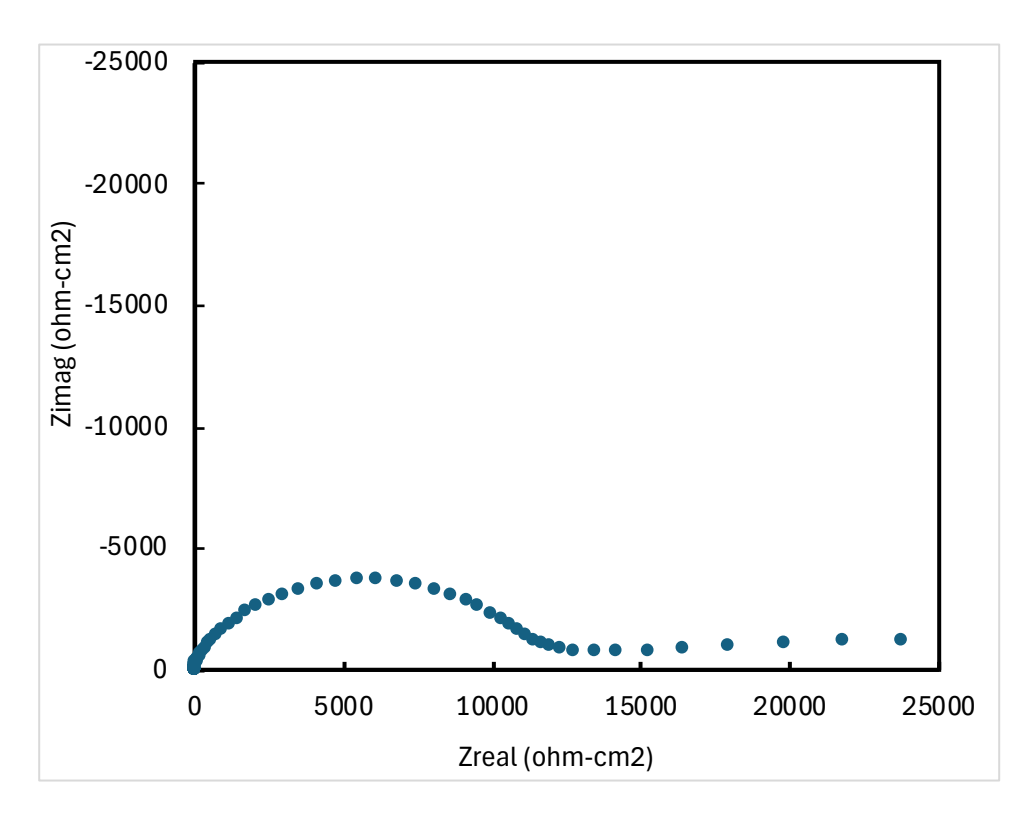
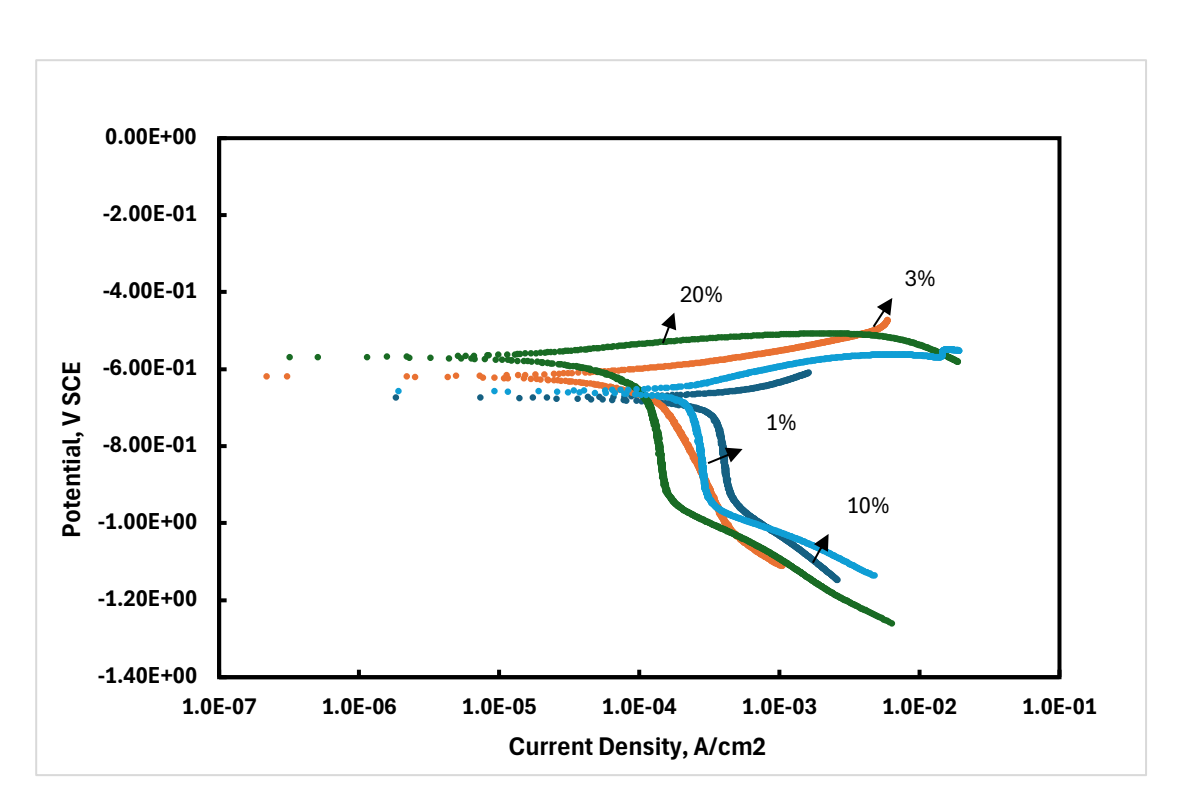
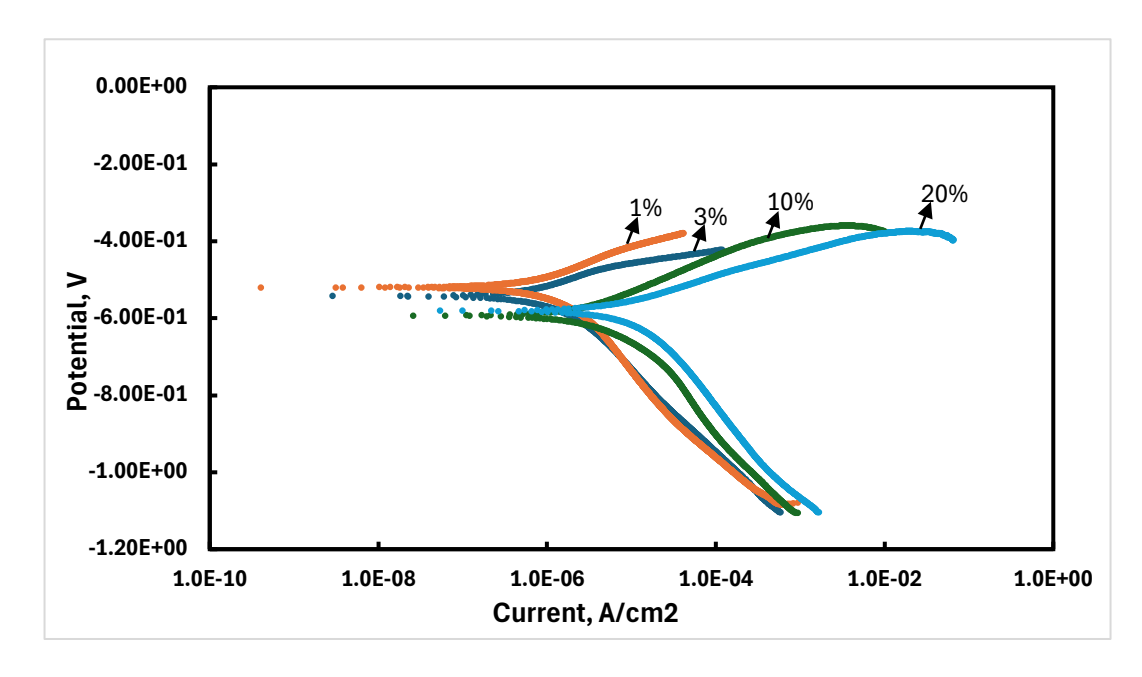


Figure 3.2.3 Typical Nyquist plot obtained from the EIS vs time data for C1018 steel in a RCE experiment. Solution was 1% NaCl and contained approximately 100 ppm RhL saturated with CO<sub>2</sub>. The data were collected over the frequency range of 100 kHz to 0.0001 Hz; in the figure, high frequencies (ω) are to the left and low frequencies are to the right.

Effect of High Saline on IE: The final task of this milestone will be making %IE measurements in produced water from the Eagle Ford oil reserve. The last task before those measurements is to evaluate the effect of high saline concentrations on %IE. These experiments investigated the effect of varying NaCl concentrations (1%, 3%, 10%, and 20%) on the corrosion behavior of carbon steel in both with and without RhL. For saline solution without RhL, the polarization curves show higher corrosion current densities at lower NaCl concentrations, indicating more severe corrosion. that is, decreasing NaCl concentration shifts to a higher i<sub>corr</sub> (**Figure 3.2.4**). This shift owes to an increase in the oxygen reduction rate. The addition of RhL significantly reduced i<sub>corr</sub>, as seen in **Figure 3.2.5**, demonstrating the protective effect of RhL. However, there was a trend in the inhibition efficiency with increased sodium chloride concentration as seen in **Figure 3.2.6**. However, the % IE is still quite high relative to other inhibitors which are typically in the range of 90%.



**Figure 3.2.4** Typical polarization curves for C1018 steel as a function of NaCl purged with CO<sub>2</sub> without RhL.



**Figure 3.2.5** Typical polarization curves for C1018 steel as a function of NaCl purged with CO<sub>2</sub> with the addition of approx. 100 ppm RhL.

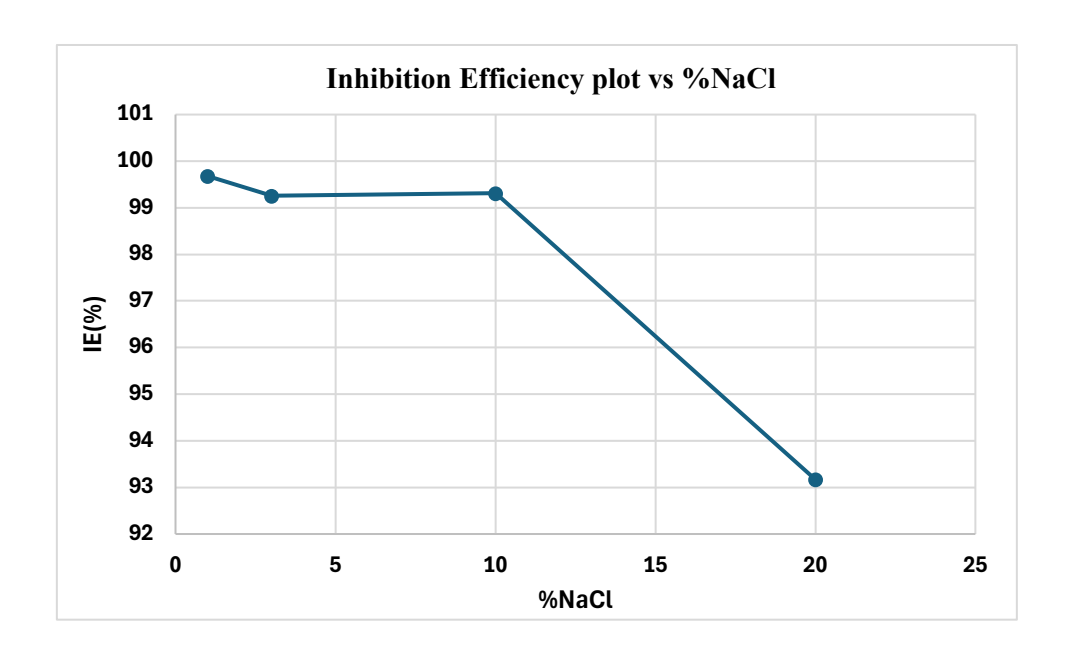


**Figure 3.2.6** RhL inhibition efficiency for C1018 as a function of NaCl concentration purged with CO<sub>2</sub>.

Adsorption Mechanism, QCM data: The final work in the PW simulant will be to learn more about the mechanism of RhL inhibition and solution properties that effect it. for RhL to inhibit corrosion of C1018, it must adsorb on the surface. One method for investigating solution properties that influence inhibition (adsorption) is the quartz crystal microbalance (QCM). The QCM measures adsorbed mass by measuring the change in resonant frequency of a coated quartz crystal (here Au on Ti). One of the first things we are measuring in these studies is RhL adsorption as a function of pH. In these experiments two buffer solutions were used, phosphate buffer with a pH of 8 and an acetic acid buffer with a pH of 4. pH was the first solution property investigated as it effects RhL micelle formation. Preliminary results from these experiments are presented in **Figure 3.2.7** where the graph plots change in resonance frequency with time. In these experiments, the baseline resonance frequency in the buffer solution was recorded for a period of time prior to the addition of RhL. Once RhL was added (approx. 1000 s pH 4, 2000 pH 8) a change (decrease) in resonance frequency was observed consistent with an increase in crystal mass. Typically, this change in mass is calculated using the Saurbrey equation, however, in this case, the decrease in resonance frequency observed in Figure 3.2.7 owes both to the mass associated with physical adsorption as well as interaction of adsorbed RhL with RhL in solution, e.g. a viscoelastic effect. This will be further addressed in future investigations and a rigorous analysis of the data in Figure 3.2.7 will be presented in FY '26.

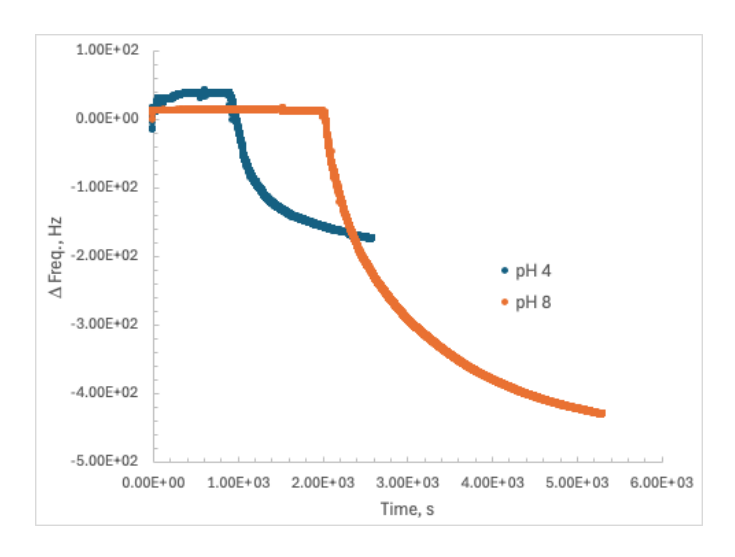


**Figure 3.2.7** QCM results showing adsorption of RhL (100 ppm) to a gold surface as a function of pH. Larger  $\Delta$ freq corresponds to a greater adsorbed mass.

#### 3.3. Task 3: MIC

*Cell Growth*: Optical density at wavelength of 600 nm was used to monitor the cell growth to identify the different growth phases for this strain. From the experiment it showed that the cells had a very high growth rate and reached the stationary phase after 24hrs.

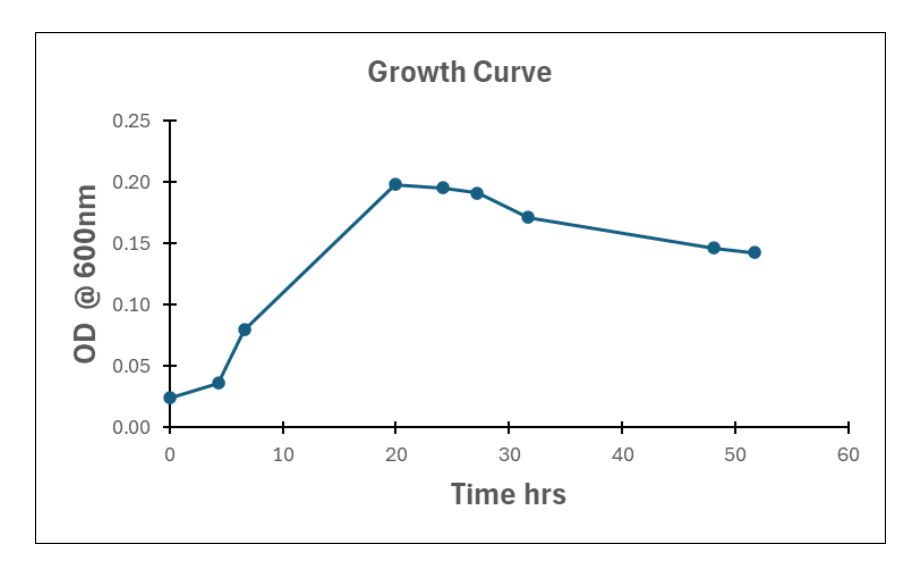


**Figure 3.3.1** Growth Curve of ATCC 7757 in ATCC 1249 Modified Baar's medium prepared in house

Modified Baar's from BTS technology was used as a quick qualitative test for sulfide production from SRB. 1 ml of an active growing SRB cells were transferred into Modified

Baar's. A serial dilution procedure was conducted on successive serum bottles to ensure that FeS was not produced, indicating the absence of sulfide in these bottles. Any sulfide production in later days will only be due to the ATCC 1249 strain. This test proved the presence of sulfate reducing bacteria.



**Figure 3.3.2:** Inoculated commercially purchased "bug bottles" for detecteing SRB activity. Left, as inoculated and Right 24hrs after inoculation showing production of sulfide in 3<sup>rd</sup> and 4<sup>th</sup> bottles.

30-day Immersion Experiments, Modified Postgate C Solution: While Postgate-C is the ideal solution to foster the growth of SRB, which is necessary to trial RhL effectiveness, it is not representative of a produced water environment. To sustain SRB while better emulating pipeline conditions, a modified version of Postgate-C was developed. The composition of this modified Postgate-C solution, hereby referred to as "Postgate-C Modified Produced Water Simulant" is shown in **Table 3.3.1**. Differences from the original Postgate-C solution include reduction of certain components and the addition of NaCl to more closely mimic the oil pipeline environment.

 Table 3.3.1: Composition of Postgate- C Modified Produced Water Simulant.

	~	
Component	Molecular Formula	Amount (g) per 1 L H <sub>2</sub> O
Sodium Chloride	NaCl	10
Sodium Pyruvate	C <sub>3</sub> H <sub>3</sub> NaO <sub>3</sub>	1.0
Sodium Sulfate	Na <sub>2</sub> SO <sub>4</sub>	0.8
Ammonium Chloride	NH <sub>4</sub> Cl	0.2
Monopotassium Phosphate	KH <sub>2</sub> PO <sub>4</sub>	0.1
Magnesium Sulfate Heptahydrate	MgSO <sub>4</sub> ·7H <sub>2</sub> O	0.1
Calcium Chloride Hexahydrate	CaCl <sub>2</sub> · 6H <sub>2</sub> O	0.1
Carbon Dioxide	CO <sub>2</sub>	Saturated

In **Figure 3.3.3**, the residue that resulted from exposure to the non-RhL solution is shown. This build-up was gel-like and had the smell of rotten eggs. This residue was somewhat removed with DI water and gentle scrubbing, but the black hardened residue remained. It si attributed to SRB activity. Upon removing the black gel-like bio film from the C1018 specimens, the non-RhL and RhL coupon surfaces were clearly different as shown in **Figure 3.3.4**. Sample 15 shows minimal corrosion product, while Sample 13 is coated in black

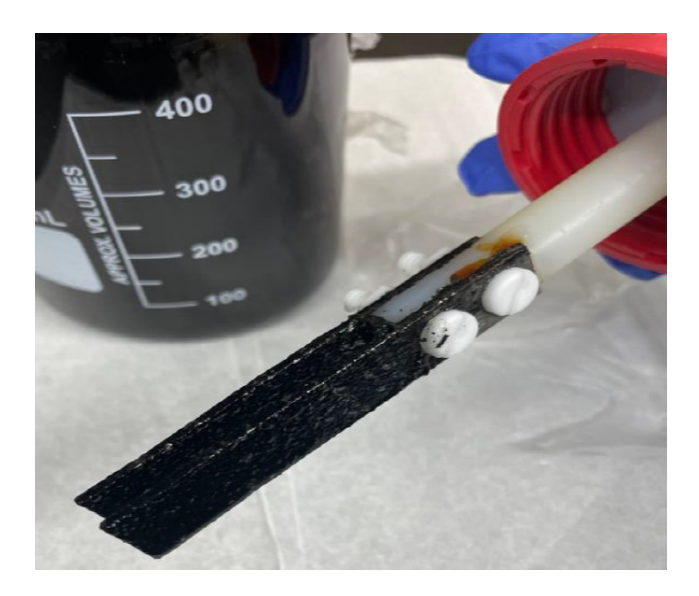


**Figure 3.3.3** Image of the coupon attachment to red bottle caps following deaeration. Two coupons were submerged in each solution, accounting for 4 coupons total in the 30-day exposure in modified Postgate-C (**Table 3.3.1**).



**Figure 3.3.4** Two examples of the coupons after the month-long exposure experiment in Postgate-C. Sample 13 (top) was submerged in the non-RhL solution while sample 15 (bottom) was submerged in the RhL solution.

### corrosion product

To determine the composition of the unidentified black residue, Scanning Electron Microscopy (SEM) and Energy-Dispersive X-ray Spectroscopy (EDS) were used. The resulting images and spectrums are shown in **Figures 3.3.5** (RhL) and **Figure 3.3.6** (non-RhL). containing oxygen, phosphorus, and sulfur. The presence of the additional elements (O, S, and P) in the non-RhL coupons suggest the formation of corrosion products such as iron oxides and iron sulfides.

The detection of sulfur and phosphorus indicates possible microbial activity, particularly

from SRB, and the presence of organic biofilm material. Although SRB was not intentionally introduced and sterile precautions were followed, the visual and analytical evidence indicates potential contamination. This may have occurred during solution preparation in a shared lab where SRB was being cultivated. To prevent further contamination, the equipment used in this trial was not used in future experiments.

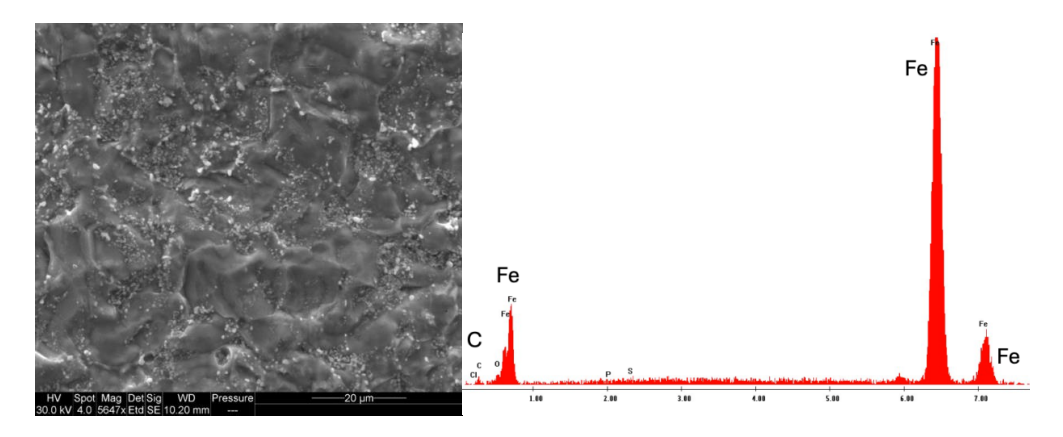


**Figure 3.3.5** Image taken using a Scanning Electron Microscope (SEM) of Sample 15, a RhL sample, at 5647X magnification. The spectrum that resulted from an EDS analysis on the zone to the left is also given. Iron (Fe) and carbon (C) are the only notable elements present.

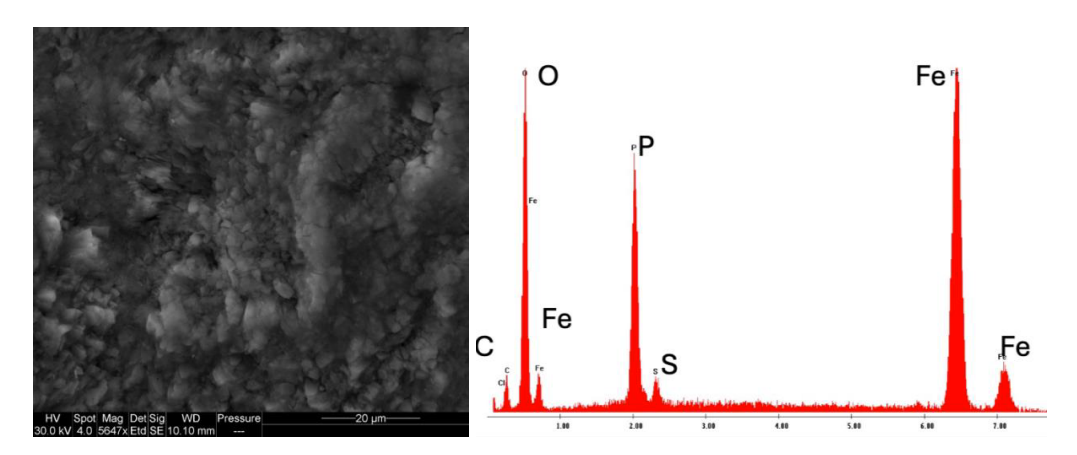


**Figure 3.3.6** Image, taken using the SEM, of Sample 13, a Non-RhL sample, at 5647X magnification. The spectrum that resulted from an EDS analysis on the zone to the left is also given. Iron (Fe), oxygen (O), phosphorus (P), sulfur (S), and carbon (C) are the notable elements present.

Postgate C Baseline Electrochemical Tests: Electrochemical tests on C1018 in Postgate C were performed so that the effects of SRB could be discerned. OCP data was collected over about 100 hours the exposure time for both cells. The OCP data found for the non-RhL solution is shown in **Figure 3.3.7**. The gap in measurements was owes to an unplanned power outage, but the final measurements, shown in pink, give a fair estimation for where the intermediate data would have fallen. The open circuit potential initial value was around -0.706 V, and the final value leveled out around -0.713 V. For comparison, OCP data for the RhL solution for about 100 hours. The OCP data found for the RhL solution is shown in **Figure 3.3.8**. As seen in this figure, the OCP for C1018 in RhL is on the order of 200 mV more positive than the non-RhL case.

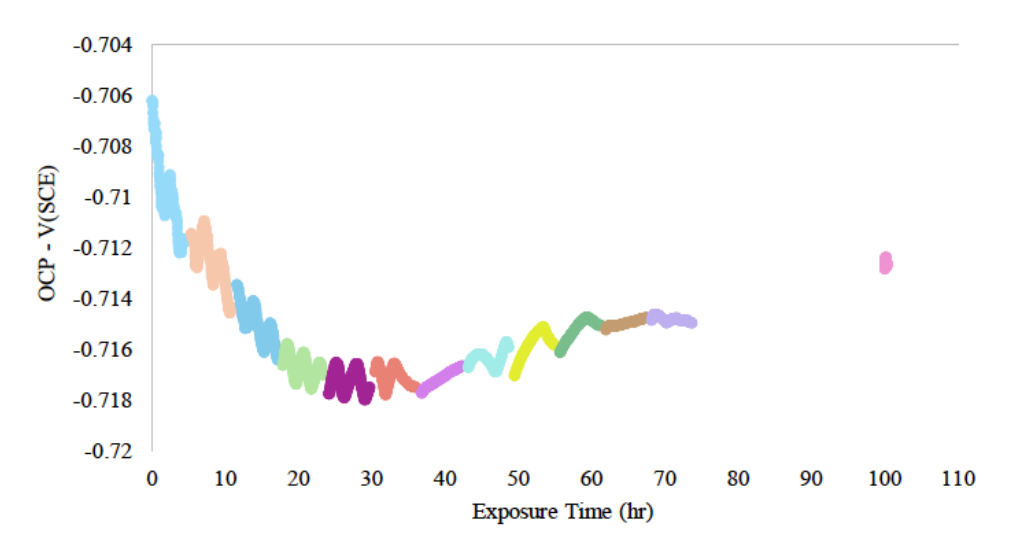


**Figure 3.3.7** The OCP data collected during the 4-day exposure experiment with the non-RhL solution. Each color represents a time segment where the OCP was measured in between LPR measurements.

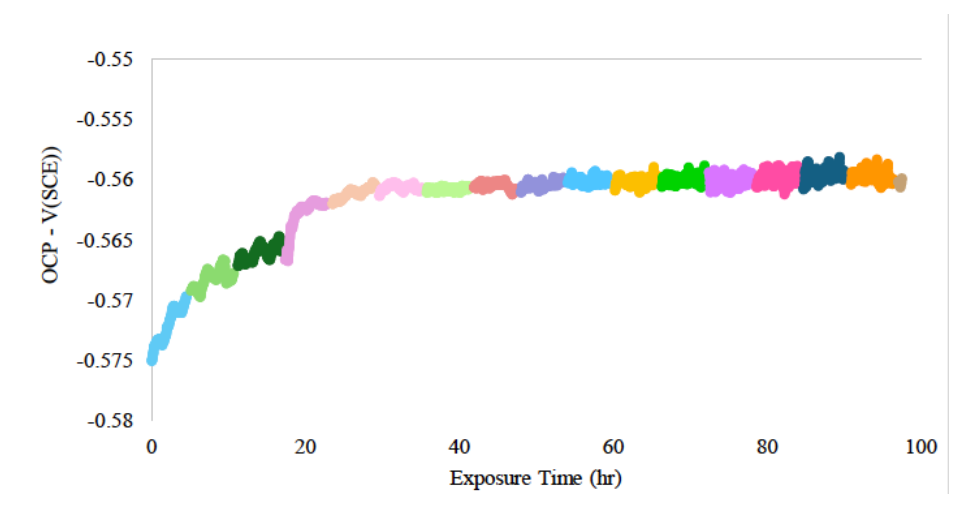


**Figure 3.3.8** The OCP data collected during the 4-day exposure experiment with the RhL solution. Each color represents a time segment where the OCP was measured in between LPR measurements.

During the course to the OCP measurements, LPR data were collected every six hours for both the RhL and non-RhL solutions. Corrosion rate was determined from the polarization curves in these solutions (data bot shown) the anodic and cathodic Tafel slopes for C1018 in each solution (**Table 3.3.2**) and Faraday's Law. The resulting data are presented in **Figure 3.3.9**. As seen in this figure, The RhL corrosion rate decreased as time increased, and the non-RhL corrosion rate increased as time increased. In addition to the difference in overall trend, the corrosion rate values for the RhL solution were multiple magnitudes smaller than those within the non-RhL solution.

**Table 3.3.2**. Tafel slopes used to calculate corrosion rate for C1018 in 1% NaCl purged with CO2 with and without RhL.

	$\beta_{a}\left(V\right)$	$\beta_{c}(V)$
non-RhL	0.104	0.500
RhL	0.107	0.249

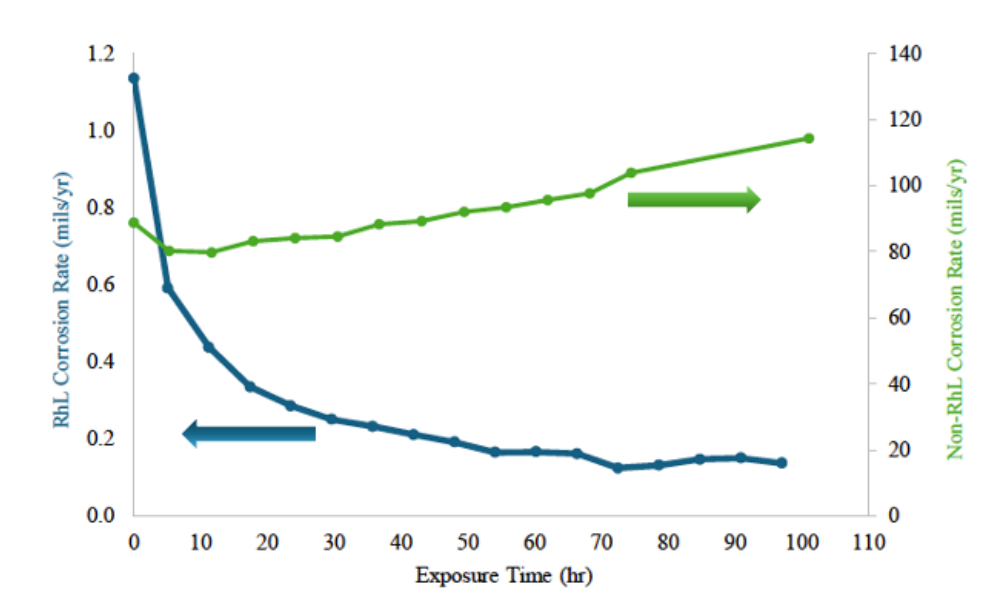


**Figure 3.3.9** Change in corrosion rate over the duration of the exposure experiment. The left y-axis shows the corrosion rate for the RhL solution. The right y-axis shows the corrosion rate for the non-RhL solution.